

Efficient Multi-Configurational Wavefunction Method with Dynamical Correlation Using Non-Orthogonal Configuration Interaction Singles and Doubles (NOCISD)

Jacob M. Nite and Carlos A. Jiménez-Hoyos*

Department of Chemistry, Wesleyan University, Middletown, CT 06459

E-mail: cjimenezhoyo@wesleyan.edu

Abstract

It is well known that inclusion of dynamical correlation is needed in order to reach quantitative agreement with experiment for molecular systems with multi-reference character. In this work, we start from a non-orthogonal configuration interaction (NOCI) framework that accounts for the static correlation and incorporate dynamical correlation by including singles and doubles excitations out of each reference determinant resulting in a NOCISD wavefunction. The equations defining the NOCISD wavefunction commonly require the solution a poorly condition generalized eigenvalue problem, which we avoid by projecting the equations to a small dimension space defined by the CISD eigenvectors of each reference determinant. We show that NOCISD results are in good qualitative agreement with other state-of-the-art method for challenging problems such as the electron transfer in the ethylene dimer radical cation and LiF, as well as the description of the Jahn-Teller distortion in the cyclopentadienyl and nitrogen trioxide radicals.

1 Introduction

While it is well understood how to properly account for the static correlation present in systems with multi-reference character, further incorporation of dynamical correlation, in a computationally efficient manner, constitutes one of the challenges in quantum chemistry. Interesting chemical systems that require a multi-reference description include, but are not limited to, molecules that undergo Jahn-Teller distortions and molecules whose reactivity is affected by the presence of conical intersections (or avoided crossings).

Most common approaches capable of producing high accuracy results in multi-reference systems build upon a multi-configuration reference space. While many methods exist for defining the configurations included in the reference space, the field is mainly dominated by the use of complete active space (CAS) wavefunctions. One benefit of CAS type reference spaces is the natural way in which one can determine the active space based on chemical intuition. However, CAS wavefunctions become intractable once the number of orbitals needed approaches 16 due to the number of configurations growing exponentially. Other approaches such as density matrix renormalization group (DMRG) techniques have been effective at reducing the computational burden of including a large number of states in the wavefunction¹. Yet another approach to formulating wavefunctions with sufficient multi-reference character while minimizing the size of the expansion has been to consider an expansion consisting of non-orthogonal determinants.

The construction of non-orthogonal configuration interaction (NOCI) wavefunctions is far from a new idea^{2,3}, but it never garnered the proliferation achieved by its orthogonal counterparts. The advantage of NOCI is that the number of determinants can be controlled *a priori*, thus enabling its use in large systems. The determinants chosen can intuitively correlate to the expected dominant configurations, such as the use of Hartree-Fock (HF) optimized excited states of a molecular system, while also incorporating orbital relaxation effects from the onset. One can further optimize the reference determinants in the presence of each other in a resonating HF-type framework⁴⁻⁷. In addition to the study of ground state

properties, NOCI based methods have also been used to study low-lying excited states using a handful of HF determinants, making the methods attractive for studying excited states of systems too large for traditional multi-references methods⁸⁻¹⁰.

While the benefits of describing complicated systems with only a handful of configurations is attractive for large molecular systems, the lack of black box selection of configurations and the increased computational complexity of NOCI based approaches have limited their widespread adoption. The main difficulty with packaging NOCI into an easy to use interface is the lack of CAS-like simplicity in terms of selection of configurations, since the major advantage of needing few configurations requires that the configurations selected capture the important aspects of the system while minimizing redundant information. New developments in finding unique non-orthogonal HF determinants for a system are improving the techniques and strategies for finding good determinants to build NOCI wavefunctions^{9,11}.

The increased computational complexity of non-orthogonal based approaches becomes evident as one intends to perform correlated calculations using the NOCI wavefunction as a reference. While NOCI based wavefunctions can, if properly constructed, easily account for the static correlation, the lack of significant dynamic correlation in NOCI wavefunctions limits their applications to qualitative comparisons. Just as in CAS-based approaches, inclusion of dynamic correlation is necessary to reach quantitative agreement with experimental results. Previous attempts to add dynamic correlation have focused on a second-order perturbation theory correction to the NOCI wavefunction¹²⁻¹⁴. We note that in those approaches the required matrix elements were evaluated using a resolution-of-the-identity approach. Due to computational constraints, higher order terms were not calculated exactly, requiring carefully constructed higher order approximation to preserve size-extensivity¹³. This is a reasonable trade-off since the calculation of higher and higher order excitation terms can quickly negate any computational saving brought about by the use of non-orthogonal determinants.

Here we present the formalism for constructing wavefunctions accounting for dynamic

correlation by the formulation of the non-orthogonal analog of multi-reference configuration interaction (MRCI). This results in the non-orthogonal configuration interaction with singles and doubles (NOCISD). Although similar approaches have appeared before (mostly using a perturbation expansion rather than a diagonalization approach), we calculate matrix elements between non-orthogonal determinants using Wick’s theorem rather than using a resolution-of-the-identity approach. While this method can be formulated to include any number of higher excitation states, here we truncated at doubles for computational efficiency. To assess the utility of this approach, we have compared NOCISD to other orthogonal multi-reference methods on small molecule systems with interesting ground and excited state potential energy surfaces.

2 Formalism

2.1 Non-Orthogonal Configuration Interaction (NOCI)

The building block of NOCISD is the NOCI wavefunction, which takes the form

$$|\Psi\rangle = \sum_{\alpha} f^{\alpha} |\Phi^{\alpha}\rangle, \tag{1}$$

where $\{f\}$ is the set of linear coefficients obtained from the diagonalization of the Hamiltonian among the determinants $\{\Phi\}$. The determinants $\{\Phi\}$ in the expansion are in general non-orthogonal, i.e., $\langle\Phi_i|\Phi_j\rangle \neq 0$. In principle one can work with an arbitrary set of determinants, though in this work we use determinants $\{\Phi\}$ that constitute HF solutions, i.e., they are stationary points of the HF energy functional.

2.2 Non-Orthogonal Singles and Doubles Expansion

In order to account for dynamic electron correlation we expand the NOCI wavefunction to include all possible singles and doubles excitations from the reference determinants, similar

in spirit to the how MRCI constitutes an expansion from a reference MC-SCF wavefunction. The NOCISD wavefunction then takes the form

$$|\Psi\rangle = \sum_{\alpha} f^{\alpha} |\Phi^{\alpha}\rangle + \sum_{\alpha} \sum_{i,a} (f^{\alpha})_i^a |(\Phi^{\alpha})_i^a\rangle + \sum_{\alpha} \sum_{i<j,a<b} (f^{\alpha})_{ij}^{ab} |(\Phi^{\alpha})_{ij}^{ab}\rangle. \quad (2)$$

Here, i, j label occupied orbitals and a, b label virtual orbitals. The coefficients f^{α} , $(f^{\alpha})_{i,a}$, and $(f^{\alpha})_{ij,ab}$ are determined from the ground state solution to the generalized eigenvalue problem

$$\mathbf{H}\mathbf{F} = \mathbf{S}\mathbf{F}\varepsilon, \quad (3)$$

where \mathbf{H} is the Hamiltonian matrix, \mathbf{S} is the overlap matrix, and \mathbf{F} and ε are the matrices of eigenvectors and eigenvalues, respectively. Naturally, the solution to Eq. 3 also provides access to low-energy excited states with a wavefunction analogous to that in Eq. 2. In this work, we use Wick’s theorem (see appendix) to evaluate all the required overlap and Hamiltonian matrix elements.

2.3 Practical Implementation

Given a set of non-orthogonal reference determinants, the NOCISD wavefunctions and energies are obtained by solving the generalized eigenvalue problem of Eq. 3. A direct solution of Eq. 3 is difficult due to the typically large dimension of the matrices and the fact that the overlap matrix can easily develop near or exact singularities.

Iterative approaches to Eq. 3 rely on solving the linear equation problem $\mathbf{S}x = b$ or a related one. We have found that many of the common iterative algorithms converge slowly when \mathbf{S} is poorly conditioned. In most of our test cases, the large dimension of the NOCISD matrices yield overlap matrices with many small eigenvalues. We note that the direct removal of all small eigenvalues of \mathbf{S} by a diagonalization of the full matrix is impractical given the typical dimensions of the NOCISD problem.

We have therefore opted for a contracted scheme: rather than attempting a direct so-

lution to Eq. 3, we use only the lowest n eigenvectors and eigenvalues of the standard CISD problem (with n being small) associated with each reference determinant. The CISD problems are easier to solve with a conventional Davidson algorithm¹⁵ given that they are standard eigenvalue problems. We then transform Eq. 3 to the small basis of $n \times m$ CISD eigenvectors, with m being the number of reference determinants. A full solution to the generalized eigenvalue problem in the small basis is then feasible.

3 Computational Details

We discuss in the next section calculations on LiF, C₅H₅, NO₃, fulvene, and the ethylene dimer radical cation. Unless otherwise noted, Gaussian 16¹⁶ was used to carry out geometry optimizations using an unrestricted HF (UHF) wavefunction and to perform state-specific and state-averaged (SA) CASSCF calculations.

The reference determinants used in the NOCI expansion were obtained using an in-house code using a Newton-Raphson algorithm to find HF solutions. The use of Newton-Raphson avoids collapse to the lowest energy determinant, thereby allowing us to have several reference determinants for each system.

Our NOCISD calculations were done using a Python code that retrieves integrals from Gaussian 16 via its Python interface. We solve each CISD eigenvalue problem using the PRIMME iterative eigenvalue problem library^{17,18}. Our current code requires us to hold all two-electron integrals in memory, which prevents us from using large basis sets. We use the cc-pVDZ basis set for calculations on C₅H₅, NO₃, and fulvene. While this is a rather small basis set, it is sufficient to allow a qualitative comparison with previous literature results on the same systems. The ethylene dimer radical cation calculations use the 6-31+G basis set to match the benchmark studies by Pieniazek *et al.*¹⁹. The LiF calculations use the custom basis used by Bauschlicher and Langhoff²⁰.

4 Results and Discussion

4.1 Ethylene Dimer Radical Cation

The ethylene dimer radical cation is a useful prototype model for electron transfer reactions. The stable formation of the dimer combined with the modest computational requirements needed has made the $(\text{C}_2\text{H}_4-\text{C}_2\text{H}_4^+)$ system ideal for benchmarking electronic structure methods used to study electron transfer mechanisms. In this work, we focus on the parallel stacked orientation to test the quality of NOCISD potential energy curves in the electron transfer process between monomers.

The reaction coordinate (RXC) used for the $(\text{C}_2\text{H}_4)_2^+$ system follows the procedure outlined by Pieniazek *et al.*¹⁹ Briefly, a linearly interpolated RXC was constructed from independently optimized C_2H_4 and C_2H_4^+ structures. The monomers were arranged in two parallel π -stacked configurations ($\text{C}_2\text{H}_4 - \text{C}_2\text{H}_4^+$ and $\text{C}_2\text{H}_4^+ - \text{C}_2\text{H}_4$) with a fixed intermolecular distance, and a linearly interpolated RXC was formed from the two configurations. The structures of C_2H_4 and C_2H_4^+ match those of Pieniazek *et al.* The determinants used in the NOCI expansion correspond to UHF solutions where the charge is localized in either of the fragments.

As discussed above, our practical implementation of NOCISD proceeds by choosing a number n of eigenvectors retained out of the CISD problem for each reference determinant. The exact NOCISD solution is recovered as n tends to the dimension of each CISD matrix. Table 1 tabulates the dependence of the NOCISD energy with respect to the number of eigenvectors retained for the $(\text{C}_2\text{H}_4)_2^+$ system at $\text{RXC}=0.5$. In this case, using only $n=2$ yields the converged NOCISD energies with sub-milliHartree accuracy. We used $n=1$ in this system as the changes in the plots in Fig. 1 are minimal when increasing to $n=2$.

Figure 1 shows the CISD and NOCISD energies along the RXC. Naturally, the CISD profiles correspond to the two crossing solutions while NOCISD couples them to yield the expected avoided crossing. At 6 Å, the diabatic CISD curves are close to the adiabatic NO-

CISD ones when RXC is close to 0 or 1. On the other hand, at 4 Å the coupling is substantial along the entire RXC. The coupling energy depends strongly interfragment separation: at 6 Å, the coupling energy at RXC= 0.5 is only 0.76 mHartree while it is 6.71 mHartree at 4 Å.

Comparing the NOCISD results to previous studies in the literature, other computational methods are in agreement with the monomer distance dependence of the dimer stabilization energy. Compared to the EOM-IP-CCSD, EOM-IP-CC(2,3), and MR-CISD+Q calculations by Pieniazek et al¹⁹, the NOCISD absolute energies are higher by ≈ 50 mHartree. However, the shape of the potential energy surface along the reaction coordinate, and the well depth of the NOCISD ground state of 1.96 mHartree compare favorably with the EOM-IP-CC(2,3) and MR-CISD+Q energies of 2.26 mHartree and 2.05 mHartree respectively.

Table 1: NOCISD energies (in a.u.) of the ground (E_0) and excited (E_1) states of the ethylene dimer radical cation at 4 Å and RC= 0.5 as a function of the number of CISD eigenvectors n retained per reference determinant.

n	E_0	E_1
1	-156.03511503	-156.01353058
2	-156.03534128	-156.01410873
15	-156.03534131	-156.01410874
30	-156.03534342	-156.01411123
45	-156.03535089	-156.01411401
60	-156.03535129	-156.01411442

4.2 Lithium Fluoride

Lithium fluoride (LiF) has long been used as a prototype system to study avoided crossings and electron transfer. Bauschlicher *et al.*²⁰ mapped out the potential energy surface using full configuration interaction (FCI) calculations; such results have become a benchmark against which approximate methods can be validated.

In our work, we study the energy profile of LiF as a function of bond distance near the expected avoided crossing. We used three determinants in the NOCI expansion: the

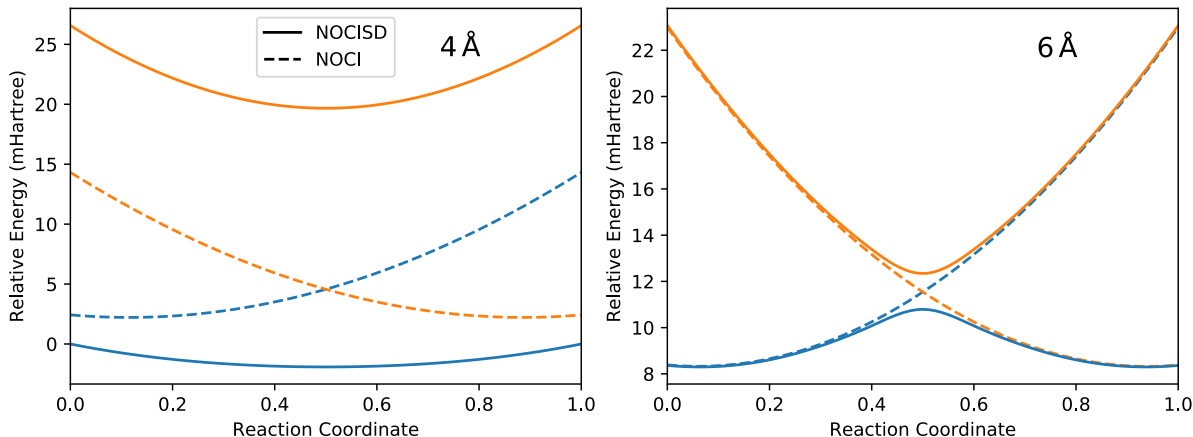


Figure 1: CISD and NOCISD absolute energies for the ground and excited states along the reaction path corresponding to electron transfer from neutral C_2H_4 to $C_2H_4^+$ for dimer separation distances of 4 Å (left) and 6 Å (right).

restricted HF (RHF) solution which dissociates into ionic fragments, and two UHF solutions (with opposite spin alignments) which dissociate into neutral fragments. We scanned the Li–F bond length from 3.3 Å to 8 Å as our reaction coordinate; we note that the UHF solution becomes unstable (and does not smoothly evolve into the RHF solution) for bond distances shorter than 3.3 Å.

In Figure 2, the relative ground state energy curves are compared for NOCI and NOCISD (using $n = 1$) as well as FCI and SA-CASSCF and SA-MRCI. Here, SA-CASSCF and SA-MRCI results from Ref.²⁰ use the (2,2) minimal active space. We would like to stress that in Ref.²⁰ the use of state averaging was found to be critical in CASSCF and MRCI calculations (see, for instance, Fig. 4).

As expected, methods which include dynamic correlation have closer agreement to the FCI curve compared to the methods without (CASSCF and NOCI). Qualitatively, the SA-MRCI curve has the closest agreement with FCI. The CISD curve has an incorrect curvature past 6 Å which reflects the inappropriate nature of the RHF reference for large bond lengths. We note that the FCI and SA-MRCI results from Ref.²⁰ were carried out using a frozen core approximation, complicating a direct comparison between our NOCISD results and FCI.

Examining the difference between the NOCI and NOCISD LiF curves (see Fig. 3) high-

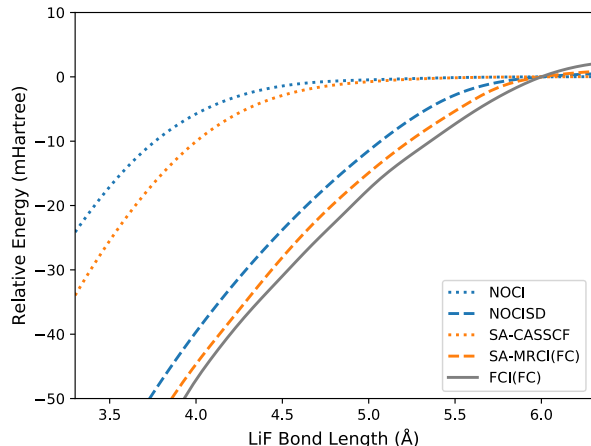


Figure 2: Ground state energies of LiF (relative to the energy at 6 Å) as a function of the Li–F bond distance. FCI, CAS, and MRCI data is adapted from Ref.²⁰.

lights the improvement due to the inclusion of dynamic correlation to the NOCI wavefunction. Comparing the set of curves representing those wavefunctions without dynamic correlation (the HF curves and NOCI curves) vs those with dynamic correlation (CISD and NOCISD curves), both sets show the expected diabatic vs adiabatic curves for the independent wavefunctions and non-orthogonal wavefunctions respectively. The diabatic crossing point for the HF curves is about 3.6 Å while the CISD curves cross at ≈ 5.5 Å. By allowing the separate wavefunctions to mix in the NOCI based wavefunction, the expected avoided crossing develops near the diabatic crossing point. The NOCISD curves very closely follow the CISD curves except in the small region near the crossing point, compared to the NOCI curves which have a large section where the NOCI curves deviate from the HF solutions. Note also that using $n = 2$ in NOCISD calculations only changes the excited state profile (with respect to $n = 1$) at short Li–F bond lengths; using larger n only changes the energy profiles minimally.

Compared to experimental estimates as well as FCI and SA-MRCI (with larger active spaces) calculations, the NOCISD crossing point is underestimated by up to 1.6 Å. Looking at the dipole moment as a function of bond length (see Fig. 4), the NOCISD (using $n = 1$) curve is shifted left of the SA-MRCI curve by 0.5 Å (a similar shift is seen between the NOCI and SA-CASSCF curves). Comparing the SA-CAS/SA-MRCI dipole moment curves with

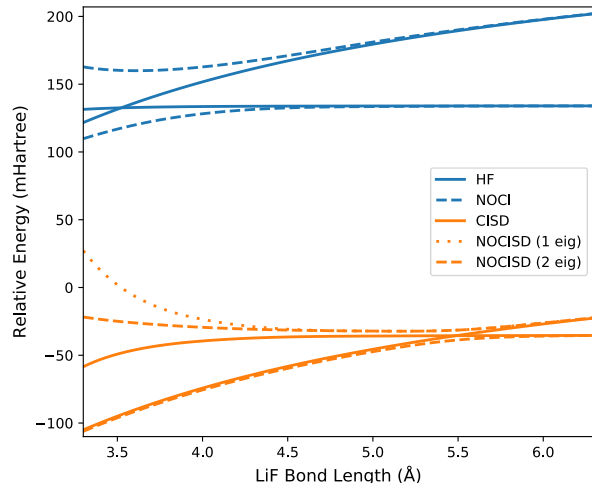


Figure 3: NOCI and NOCISD (with $n = 1$ and $n = 2$) energies as a function of the Li–F bond distance. The energies are plotted relative to the RHF energy at equilibrium.

the NOCI/NOCISD curves, the NOCI gives similar behavior to SA-CAS. Adding single and double excitations to both CAS and NOCI gives similar improvements. From the energy and dipole moment curves, the NOCISD method captures a significant portion of the correlation missing from the NOCI wavefunction. Obtaining NOCISD curves that better match the experimental crossing point clearly need more than the two determinants used in the NOCI expansion, similar to the improvement seen in the previous of the MRCI dipole moment curves upon use of larger active spaces²⁰.

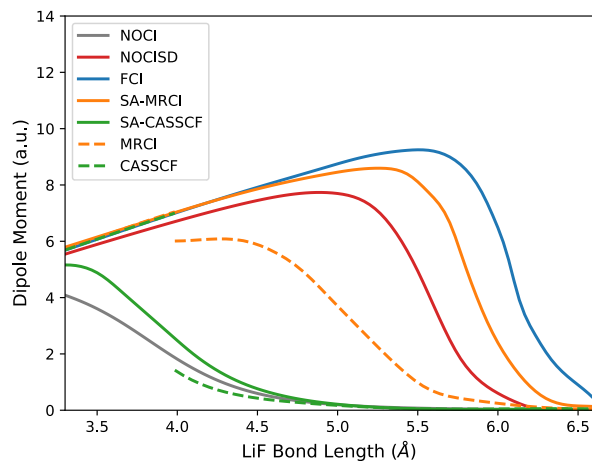


Figure 4: Dipole moment of LiF as a function of Li–F bond distance with various methods. FCI, CAS, and MRCI data is adapted from Ref.²⁰.

4.3 Cyclopentadienyl Radical

The cyclopentadienyl radical has attracted experimental and theoretical interest over half a century due to its central role for understanding π -conjugated systems. The Jahn-Teller distortion along a C_2 axis of the molecule has been the center of investigations into the equilibrium structure of the radical as well as the nature of the vibrational modes contributing to the Jahn-Teller distortion (see, for instance, Refs.²¹⁻²³).

In this work we study the cyclopentadienyl radical along a Jahn-Teller distortion coordinate. We start by converging the UHF equilibrium geometry under both D_{5h} and C_{2v} symmetries. In the latter case, one can find five different such geometries with distortion along different C_2 axis. In order to produce our reference set of determinants, we drive each of the five different solutions back to the symmetric D_{5h} structure. We then proceed to take each of those five UHF solutions and distort along a given C_2 axis; this constitutes our reaction coordinate (RXC). The use of the Newton-Raphson optimization is crucial to avoid collapse to the lowest-energy HF solution. We cannot drive all five different solutions along RXC to completion: solutions start to collapse down for large values of RXC. We thus only study from RXC= 0 (the D_{5h} structure) to RXC= 0.4 (2/5 of the way to the fully distorted UHF C_{2v} structure).

As shown in Fig. 5, at the D_{5h} symmetric configuration CISD yields a non-degenerate ground state and leads to a lowest excitation energy of ≈ 600 mHartree. This is in sharp contrast to a SA-CASSCF (5,5) calculation which yields 5 low energy states, closely reproduced by NOCI. Upon inclusion of dynamical correlation in NOCISD, the shape of the low-energy spectrum is mostly preserved: a doubly degenerate ground state (of E'' symmetry) with low-lying excitations of ≈ 150 mHartree (A symmetry) and ≈ 200 mHartree (E' symmetry). This indicates that dynamic correlation only has a minor impact in the low-lying excitation energies. We also note that $n = 10$ is sufficient to converge the excitation energies, while $n = 1$ predicts excitation energies that are ≈ 30 mHartree too high.

The NOCI, NOCISD (using $n = 10$), and SA-CASSCF energy profiles along the Jahn-

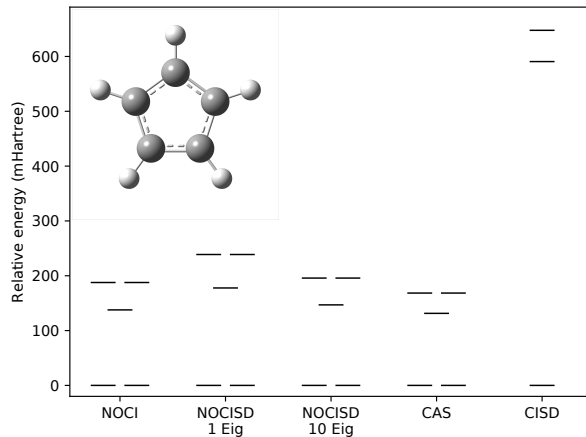


Figure 5: Low-energy spectrum of the cyclopentadienyl radical at the symmetric D_{5h} structure predicted with different methods.

Teller distortion pathway are shown in Fig. 6. The relative spacing, splitting, and curvature of each NOCI follows the lowest five NOCISD states. Upon closer inspection, we note that NOCI predicts a minimum in the ground state profile at $RXC=0.3$ while NOCISD predicts a minimum for larger RXC (beyond $RXC=0.4$). The SA-CASSCF ground state profile shows a minimum at $RXC=0.9$. At $RXC=0.4$ SA-CASSCF, NOCI, and NOCISD only display slight differences in their Jahn-Teller stabilization energies of 5.06, 3.30, and 1.35 mHartree, respectively. The low-energy scale of the ground state profile suggests that even higher-level methods may be required to yield a quantitative prediction of the Jahn-Teller distortion energy.

Figure 6 also demonstrates differing excited state behavior between the non-orthogonal methods and the CAS calculation: the SA-CASSCF excitation energies are lower than the non-orthogonal methods and exhibit smaller changes along the distortion pathway. Interestingly, both NOCI and NOCISD excitation energies show a significant increase near $RXC=0.4$, possibly indicating the need for even more reference determinants with large RXC . The experimental excitation of the transition $\tilde{A}^2A \leftarrow \tilde{X}^2E''$ is $29\,572\text{ cm}^{-1}$ ²⁴ while the NOCI, NOCISD, and SA-CASSCF excitation energies at the D_{5h} structure are $30\,229$, $32\,236$, and $28\,840\text{ cm}^{-1}$, respectively. Ignoring the zero point energy contribution in the experimental value as well as any Jahn-Teller distortions, the theoretical excitation values

are in qualitative agreement with experimental observations.

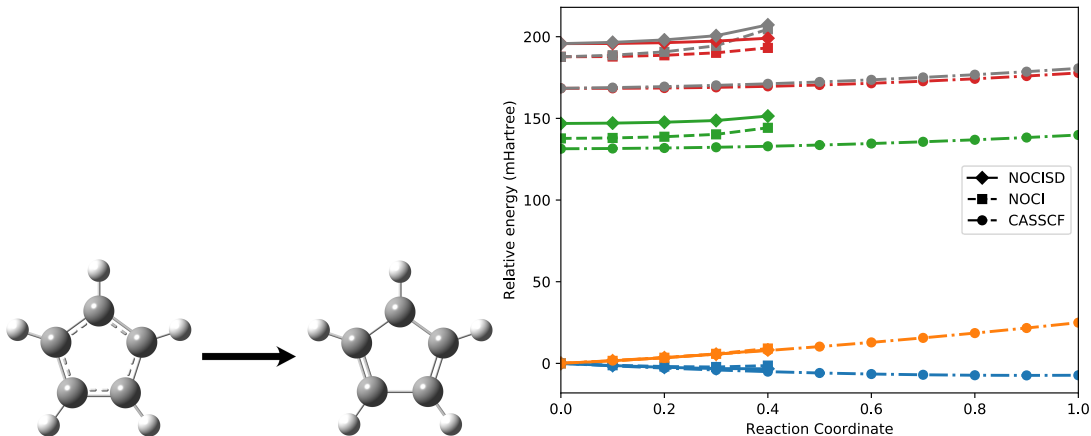


Figure 6: SA-CASSCF (5,5), NOCI, and NOCISD energies (relative to the D_{5h} structure) along the Jahn-Teller distortion pathway to the C_{2v} UHF structure of the cyclopentadienyl radical.

4.4 Fulvene

Due to its lack of radiative decay upon excitation, fulvene has been used as a prototypical system to study conical intersections (CI). Two separate geometric distortion motifs have been identified associated with intersection: the stretching of the ethyl group attached to the apex of the cyclopentane ring and the torsional rotation between the ring and ethyl group²⁵. The combination of these distortions lead to the formation of a conical intersection seam. For the purposes of this paper, we have limited our study of this system to the planar geometry, leading to a single conical intersection.

To facilitate comparison with the literature, we have chosen to use the CASSCF/cc-pVDZ structures for the S_0 and S_1 minima and the planar CI from the work of Deeb and coworkers²⁶. In our calculations we sample the paths $S_0 \rightarrow S_1$, $S_1 \rightarrow \text{CI}$, and $\text{CI} \rightarrow S_0$ by a linear interpolation of the structures.

Our NOCI calculations use four different reference determinants. The lowest-energy UHF solution on the S_0 (or the S_1) structure has a frustrated anti-ferromagnetic spin arrangement with an unfavorable ferromagnetic interaction between carbons 5 and 1 (see Scheme 7).

Three degenerate, symmetry-related determinants can be formed by the combination of a C_2 operation on the solution and a spin flip.

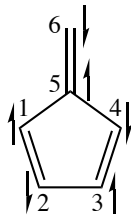


Figure 7: Fulvene structure with UHF placement of unpaired electrons shown as arrows.

Previous studies on fulvene have characterized the S_1 equilibrium structure as a shallow minimum²⁵. CAS-MP2 calculations with a (6,6) active space yields similar features to previous CASSCF results with the S_1 state having excitation energies of 60.8 and 61.2 kcal/mol respectively and the CI having an excitation energy of 66.8 and 69.4 kcal/mol, respectively. The NOCISD curves for the S_1 state lack the local minimum at the S_1 geometry, and instead have a smooth downward path towards the CI. The excitation energies of the 1B_1 at the S_1 and CI geometries with respect to the 1A_1 state at the S_0 geometry are 76.5 and 67.1 kcal/mol respectively. The NOCISD wavefunction reproduces many of the important features of the planar fulvene system, including the conical intersection. We note that in this case $n = 4$ determinants are needed to converge the NOCISD potential energy surfaces, particularly the S_1 energy near the S_0 structure.

4.5 Nitrogen Trioxide

The nitrogen trioxide radical has been the focus of many studies due to its importance in atmospheric chemistry. The electronic structure of the ground state has been controversial for some time. Early theoretical studies found a C_{2v} distorted structure as the minimum structure of NO_3 rather than a D_{3h} structure (see, for instance, Ref.²⁷).

The ground state potential energy profile between the D_{3h} and C_{2v} structures of NO_3 has been found from previous ab initio calculations to be very flat^{27–29}. Careful ground state studies by Einfeld and Morokuma have lead to the current consensus that the D_{3h} geometry

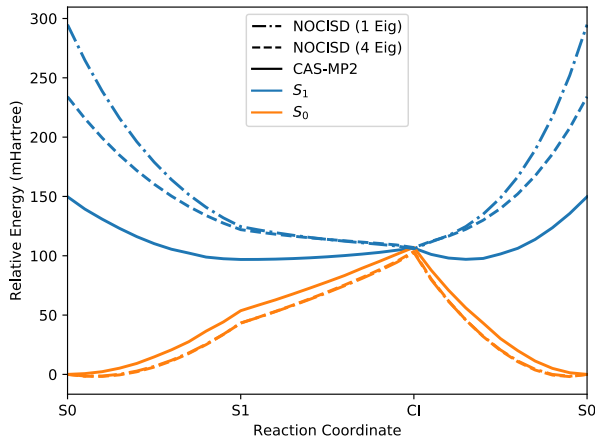


Figure 8: NOCISD (using $n = 1$ and $n = 4$) and CAS-MP2 energies along the linearly interpolated path $S_0 \rightarrow S_1 \rightarrow \text{CI} \rightarrow S_0$. The energies are relative to the S_0 energy at the S_0 structure.

is the equilibrium structure^{29,30}.

As with cyclopentadienyl radical, we used UHF optimized structures under D_{3h} and C_{2v} symmetry to define the Jahn-Teller distortion pathway. We obtained three different UHF solutions (by following the lowest-energy solutions along the different C_2 distortion axis), which were used as the reference determinants in the NOCI calculations. Just as in the case of C_5H_5 , we were unable to drive all HF determinants to $\text{RXC} = 1$, and therefore only sample from $\text{RXC} = 0$ to $\text{RXC} = 0.6$.

The NOCISD ground state potential energy surface along the distortion pathway (see Fig. 9) is in agreement with previous calculations in that the curve is nearly flat. NOCISD predicts the D_{3h} structure to be a minimum along the distortion pathway, consistent with previous CCSD, CCSD(T), and MRCI calculations^{28,29,31}. Just as in the case of C_5H_5 , $n = 4$ is needed to converge the low-energy spectrum as RXC gets large. In Fig. 9 we also show SA-CASSCF (5,4) calculations which incorrectly predict a fairly large stabilization energy: a significantly larger active space and inclusion of dynamical correlation is required to yield a nearly flat potential energy along the distortion pathway.

Experimentally, there are two known low energy excitations with E' and E'' symmetry. For the E' state, the NOCISD excitation energy is 74.2 mHartree. This compares well with

MRCI+Q and EOM-CC energies of 74.9 mHartree and 74.2 mHartree respectively³². We do not report NOCISD results for the E'' state as those are not available in NOCI: only three reference determinants were used. It would then be appropriate to extend the reference determinant selection to appropriately sample states of E'' symmetry.

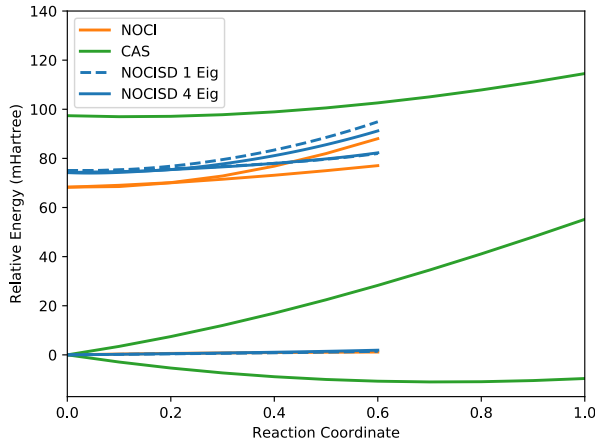


Figure 9: NOCISD ($n = 1$ and $n = 4$) and SA-CASSCF (5,4) energies with respect to the Jahn-Teller distortion pathway from the D_{3h} to the C_{2v} structure in NO_3 .

5 Conclusions

This work discusses the extension of NOCI, by inclusion of singles and doubles excitations, to account for dynamical correlation in multireference systems. The inclusion of dynamical correlation can be crucial to obtain results that agree quantitatively with experimental results or higher level calculations, as shown in the case of LiF.

Solving for the low-energy spectrum of the NOCISD Hamiltonian required the use of a contracted strategy where we first solve for n eigenstates of each reference determinant. This results in a perturb-then-diagonalize (though not really “perturb”) framework where the coefficients of the reference determinants are readjusted in the presence of dynamical correlation. In most of the cases studied, a very small n yielded converged results, implying that it is mainly the coupling of the first few CISD eigenvectors that determine the shape of the low energy spectrum. Yet this is not guaranteed for most systems.

In some of the systems studied it is clear that the reference determinants used are still not sufficient to really achieve quantitative agreement with higher-level results. The use of even more NOCI determinants, as well as a state-averaged strategy to obtain those determinants, are current avenues of investigation in our laboratory.

Overall, we find that NOCISD can yield results of comparable accuracy to MRCI. We think that there are a number of systems where NOCI can be more useful as a zeroth-order reference than CAS as it avoids the exponential wall associated with the latter. Just as MRCI, the diagonalization approach used in NOCISD is not size extensive. As proven by the commonplace use of MRCI, this detrimental feature need not render NOCISD as a useless method.

6 Appendix

In this appendix we briefly discuss how the evaluation of matrix elements of the NOCISD Hamiltonian can be carried out.

We start with the Hamiltonian \hat{H} written as

$$\hat{H} = \sum_{\mu\lambda} h_{\mu\lambda} a_{\mu}^{\dagger} a_{\lambda} + \frac{1}{4} \sum_{\mu\nu\lambda\sigma} \langle \mu\nu | v | \lambda\sigma \rangle a_{\mu}^{\dagger} a_{\nu}^{\dagger} a_{\sigma} a_{\lambda} \quad (4)$$

where h and v are the tensors of one- and (antisymmetrized) two-electron integrals respectively and a and a^{\dagger} are creation and annihilation operators. We assume in what follows that an orthonormal basis is used. It is well known³³ that Wick's theorem can be applied in the evaluation of matrix elements between two non-orthogonal determinants $|\Phi_{\text{L}}\rangle$ and $|\Phi_{\text{R}}\rangle$ (i.e., $\langle \Phi_{\text{L}} | \Phi_{\text{R}} \rangle \neq 0$). All the non-vanishing contractions can be expressed in terms of the transition density matrix $\rho^{\text{L,R}}$ defined as

$$\rho_{\lambda\mu}^{\text{L,R}} \equiv \frac{\langle \Phi_{\text{L}} | a_{\mu}^{\dagger} a_{\lambda} | \Phi_{\text{R}} \rangle}{\langle \Phi_{\text{L}} | \Phi_{\text{R}} \rangle}. \quad (5)$$

Explicit expressions for overlap and Hamiltonian matrix elements between two non-

orthogonal determinants $|\Phi_L\rangle$ and $|\Phi_R\rangle$ are provided below. Let C_L be the (rectangular) $M \times N$ matrix of occupied orbitals in $|\Phi_L\rangle$ and C_R be the corresponding set of occupied orbitals in $|\Phi_R\rangle$. Similarly, let D_L and D_R be the (rectangular) $M \times (M - N)$ matrices of virtual orbitals in $|\Phi_L\rangle$ and $|\Phi_R\rangle$. Overlap and Hamiltonian matrix elements are given by

$$s_{L,R} \equiv \langle \Phi_L | \Phi_R \rangle = \det X, \quad (6)$$

$$h_{L,R} \equiv \frac{\langle \Phi_L | \hat{H} | \Phi_R \rangle}{\langle \Phi_L | \Phi_R \rangle} = \frac{1}{2} \text{Tr} [\rho^{L,R} (h + F^{L,R})], \quad (7)$$

with $X = C_L^\dagger C_R$ and with $\rho^{L,R}$ and $F^{L,R}$ evaluated as

$$\rho^{L,R} = C_R X^{-1} C_L^\dagger, \quad (8)$$

$$F_{\mu\lambda}^{L,R} = h_{\mu\lambda} + \sum_{\nu\sigma} \langle \mu\nu | v | \lambda\sigma \rangle \rho_{\sigma\nu}^{L,R}. \quad (9)$$

The evaluation of matrix elements between excited determinants can also make use of Wick's theorem. For example, the overlap between $|\Phi_L\rangle$ and $|(\Phi_R)_{mn}^{ab}\rangle$ is given by

$$\frac{\langle \Phi_L | (\Phi_R)_{mn}^{ab} \rangle}{\langle \Phi_L | \Phi_R \rangle} = \sum_{\mu\nu\lambda\sigma} (C_R)_{\mu a} (C_R)_{\lambda m}^* (C_R)_{\nu b} (C_R)_{\sigma n}^* [\rho_{\lambda\mu}^{L,R} \rho_{\sigma\nu}^{L,R} + \rho_{\sigma\mu}^{L,R} (\mathbf{1} - \rho^{L,R})_{\lambda\nu}]. \quad (10)$$

Defining $Z = C_R^\dagger \rho^{L,R} D_R$, this can be written as

$$\frac{\langle \Phi_L | (\Phi_R)_{mn}^{ab} \rangle}{\langle \Phi_L | \Phi_R \rangle} = Z_{ma} Z_{nb} - Z_{na} Z_{mb}. \quad (11)$$

Similarly, the Hamiltonian overlap between $|\Phi_L\rangle$ and $|(\Phi_R)_{mn}^{ab}\rangle$ is given by

$$\begin{aligned} \frac{\langle \Phi_L | \hat{H} | (\Phi_R)_{mn}^{ab} \rangle}{\langle \Phi_L | \Phi_R \rangle} &= h_{L,R} [Z_{ma} Z_{nb} - Z_{na} Z_{mb}] \\ &+ Z_{ma} [V F^{L,R} W]_{nb} + Z_{nb} [V F^{L,R} W]_{ma} \\ &- Z_{na} [V F^{L,R} W]_{mb} - Z_{mb} [V F^{L,R} W]_{na} \\ &+ \sum_{\mu\nu\lambda\sigma} \langle \mu\nu | v | \lambda\sigma \rangle V_{n\mu} V_{m\nu} W_{\lambda b} W_{\sigma a}, \end{aligned} \quad (12)$$

where $V = C_R^\dagger \rho^{L,R}$ and $W = (\mathbf{1} - \rho^{L,R}) D_R$.

Acknowledgement

This work was supported by a generous start-up package from Wesleyan University. JN and CAJH acknowledge Michael Frisch from Gaussian, Inc. for useful discussions.

References

- (1) Yanai, T.; Kurashige, Y.; Mizukami, W.; Chalupský, J.; Lan, T. N.; Saitow, M. Density Matrix Renormalization Group for Ab Initio Calculations and Associated Dynamic Correlation Methods: A Review of Theory and Applications. *Int. J. Quantum Chem.* **2015**, *115*, 283–299.
- (2) Jackels, C. F.; Davidson, E. R. The Two Lowest Energy $2A'$ States of NO_2 . *J. Chem. Phys.* **1976**, *64*, 2908–2917.
- (3) Voter, A. F.; Goddard, W. A. A Method for Describing Resonance between Generalized Valence Bond Wavefunctions. *Chem. Phys.* **1981**, *57*, 253–259.
- (4) Schmid, K. W.; Zheng Ren-Rong; Grümmer, F.; Faessler, A. Beyond Symmetry-

- Projected Quasi-Particle Mean Fields: A New Variational Procedure for Nuclear Structure Calculations. *Nuc. Phys. A* **1989**, *499*, 63–92.
- (5) Fukutome, H. Theory of Resonating Quantum Fluctuations in a Fermion System Resonating Hartree-Fock Approximation. *Prog. Theor. Phys.* **1988**, *80*, 417–432.
- (6) Koch, H.; Dalgaard, E. Linear Superposition of Optimized Non-Orthogonal Slater Determinants for Singlet States. *Chem. Phys. Lett.* **1993**, *212*, 193–200.
- (7) Jiménez-Hoyos, C. A.; Rodríguez-Guzmán, R.; Scuseria, G. E. Multi-Component Symmetry-Projected Approach for Molecular Ground State Correlations. *J. Chem. Phys.* **2013**, *139*, 204102.
- (8) Jiménez-Hoyos, C. A.; Rodríguez-Guzmán, R.; Scuseria, G. E. Excited Electronic States from a Variational Approach Based on Symmetry-Projected Hartree-Fock Configurations. *J. Chem. Phys.* **2013**, *139*, 224110.
- (9) Sundstrom, E. J.; Head-Gordon, M. Non-Orthogonal Configuration Interaction for the Calculation of Multielectron Excited States. *J. Chem. Phys.* **2014**, *140*, 114103.
- (10) Nite, J.; Jiménez-Hoyos, C. A. Low-Cost Molecular Excited States from a State-Averaged Resonating Hartree-Fock Approach. *J. Chem. Theory Comput.* **2019**, *15*, 5343–5351.
- (11) Thom, A. J. W.; Head-Gordon, M. Locating Multiple Self-Consistent Field Solutions: An Approach Inspired by Metadynamics. *Phys. Rev. Lett.* **2008**, *101*.
- (12) Yost, S. R.; Kowalczyk, T.; Van Voorhis, T. A Multireference Perturbation Method Using Non-Orthogonal Hartree-Fock Determinants for Ground and Excited States. *J. Chem. Phys.* **2013**, *139*, 174104.

- (13) Yost, S. R.; Head-Gordon, M. Size Consistent Formulations of the Perturb-Then-Diagonalize Møller-Plesset Perturbation Theory Correction to Non-Orthogonal Configuration Interaction. *J. Chem. Phys.* **2016**, *145*, 054105.
- (14) Yost, S. R.; Head-Gordon, M. Efficient Implementation of NOCI-MP2 Using the Resolution of the Identity Approximation with Application to Charged Dimers and Long C–C Bonds in Ethane Derivatives. *J. Chem. Theory Comput.* **2018**, *14*, 4791–4805.
- (15) Davidson, E. R. The iterative calculation of a few of the lowest eigenvalues and corresponding eigenvectors of large real-symmetric matrices. *J. Comp. Phys.* **1975**, *17*, 87 – 94.
- (16) Frisch, M. J.; Trucks, G. W.; Schlegel, H. B.; Scuseria, G. E.; Robb, M. A.; Cheeseman, J. R.; Scalmani, G.; Barone, V.; Petersson, G. A.; Nakatsuji, H.; Li, X.; Caricato, M.; Marenich, A. V.; Bloino, J.; Janesko, B. G.; Gomperts, R.; Mennucci, B.; Hratchian, H. P.; Ortiz, J. V.; Izmaylov, A. F.; Sonnenberg, J. L.; Williams-Young, D.; Ding, F.; Lipparini, F.; Egidi, F.; Goings, J.; Peng, B.; Petrone, A.; Henderson, T.; Ranasinghe, D.; Zakrzewski, V. G.; Gao, J.; Rega, N.; Zheng, G.; Liang, W.; Hada, M.; Ehara, M.; Toyota, K.; Fukuda, R.; Hasegawa, J.; Ishida, M.; Nakajima, T.; Honda, Y.; Kitao, O.; Nakai, H.; Vreven, T.; Throssell, K.; Montgomery, J. A., Jr.; Peralta, J. E.; Ogliaro, F.; Bearpark, M.; Heyd, J. J.; Brothers, E.; Kudin, K. N.; Staroverov, V. N.; Keith, T. A.; Kobayashi, R.; Normand, J.; Raghavachari, K.; Rendell, A. P.; Burant, J. C.; Iyengar, S. S.; Tomasi, J.; Cossi, M.; Millam, J. M.; Klene, M.; Adamo, C.; Cammi, R.; Ochterski, J. W.; Martin, R. L.; Morokuma, K.; Farkas, Ö.; Foresman, J. B.; Fox, D. J. Gaussian 16 Revision B.01. Gaussian Inc. Wallingford CT 2016.
- (17) Stathopoulos, A.; McCombs, J. R. PRIMME: Preconditioned Iterative Multimethod Eigensolver—Methods and Software Description. *ACM Trans. Math. Softw.* **2010**, *37*, 1–30.

- (18) Wu, L.; Romero, E.; Stathopoulos, A. PRIMME-SVDS: A High-Performance Preconditioned SVD Solver for Accurate Large-Scale Computations. *SIAM J. Sci. Comput.* **2017**, *39*, S248–S271.
- (19) Pieniazek, P. A.; Arnstein, S. A.; Bradforth, S. E.; Krylov, A. I.; Sherrill, C. D. Benchmark Full Configuration Interaction and Equation-of-Motion Coupled-Cluster Model with Single and Double Substitutions for Ionized Systems Results for Prototypical Charge Transfer Systems: Noncovalent Ionized Dimers. *J. Chem. Phys.* **2007**, *127*, 164110.
- (20) Bauschlicher, C. W.; Langhoff, S. R. Full Configuration-interaction Study of the Ionic–Neutral Curve Crossing in LiF. *J. Chem. Phys.* **1988**, *89*, 4246–4254.
- (21) Applegate, B. E.; Miller, T. A.; Barckholtz, T. A. The Jahn–Teller and Related Effects in the Cyclopentadienyl Radical. I. The Ab Initio Calculation of Spectroscopically Observable Parameters. *J. Chem. Phys.* **2001**, *114*, 4855–4868.
- (22) Ichino, T.; Wren, S. W.; Vogelhuber, K. M.; Gianola, A. J.; Lineberger, W. C.; Stanton, J. F. The Vibronic Level Structure of the Cyclopentadienyl Radical. *J. Chem. Phys.* **2008**, *129*, 084310.
- (23) Sharma, K.; Garner, S.; Miller, T. A.; Stanton, J. F. First-Principles Calculation of Jahn–Teller Rotational Distortion Parameters. *J. Phys. Chem. A* **2019**, *123*, 4990–5004.
- (24) Yu, L.; Foster, S. C.; Williamson, J. M.; Heaven, M. C.; Miller, T. A. Rotationally Resolved Electronic Spectrum of Jet-Cooled Cyclopentadienyl Radical. *J. Phys. Chem.* **1988**, *92*, 4263–4266.
- (25) Paterson, M. J.; Bearpark, M. J.; Robb, M. A.; Blancafort, L. The Curvature of the Conical Intersection Seam: An Approximate Second-Order Analysis. *J. Chem. Phys.* **2004**, *121*, 11562–11571.

- (26) Deeb, O.; Cogan, S.; Zilberg, S. The Nature of the S1/S0 Conical Intersection of Fulvene. *Chem. Phys.* **2006**, *325*, 251–256.
- (27) Davy, R. D.; Schaefer, H. F. Is There an Absence of Threefold Symmetry at the Equilibrium Geometry of the Ground Electronic State for NO₃? *J. Chem. Phys.* **1989**, *91*, 4410–4411.
- (28) Kaldor, U. The Ground State Geometry of the NO₃ Radical. *Chem. Phys. Lett.* **1990**, *166*, 599–601.
- (29) Eisfeld, W.; Morokuma, K. A Detailed Study on the Symmetry Breaking and Its Effect on the Potential Surface of NO₃. *J. Chem. Phys.* **2000**, *113*, 5587–5597.
- (30) Stanton, J. F. On the Vibronic Level Structure in the NO₃ Radical. I. The Ground Electronic State. *J. Chem. Phys.* **2007**, *126*, 134309.
- (31) Mukherjee, B.; Mukherjee, S.; Sardar, S.; Shamasundar, K. R.; Adhikari, S. A beyond Born-Oppenheimer Treatment of Five State Molecular System NO₃ and the Photodetachment Spectra of Its Anion. *Chem. Phys.* **2018**, *515*, 350–359.
- (32) Eisfeld, W.; Morokuma, K. Ab Initio Investigation of the Vertical and Adiabatic Excitation Spectrum of NO₃. *J. Chem. Phys.* **2001**, *114*, 9430–9440.
- (33) Blaizot, J.-P.; Ripka, G. *Quantum Theory of Finite Systems*; The MIT Press: Cambridge, MA, 1985.